Behavioral/Cognitive

Data-Driven Clustering of Functional Signals Reveals Gradients in Processing Both within the Anterior Hippocampus and across Its Long Axis

John N. Thorp,[1] Camille Gasser,[1] Esther Blessing,[2] and Lila Davachi[1,3]

[1]Department of Psychology, Columbia University, New York, New York 10027, [2]Department of Psychiatry, New York University Langone Medical Center, New York University Grossman School of Medicine, New York, New York 10016, and [3]Nathan Kline Institute for Psychiatric Research, Orangeburg, New York 10962

A particularly elusive puzzle concerning the hippocampus is how the structural differences along its long anteroposterior axis might beget meaningful functional differences, particularly in terms of the granularity of information processing. One measure posits to quantify this granularity by calculating the average statistical independence of the BOLD signal across neighboring voxels, or intervoxel similarity (IVS), and has shown the anterior hippocampus to process coarser-grained information than the posterior hippocampus. This measure, however, has yielded opposing results in studies of developmental and healthy aging samples, which also varied in fMRI acquisition parameters and hippocampal parcellation methods. To reconcile these findings, we measured IVS across two separate resting-state fMRI acquisitions and compared the results across many of the most widely used parcellation methods in a large young-adult sample of male and female humans (Acquisition 1, $N = 233$; Acquisition 2, $N = 176$). Finding conflicting results across acquisitions and parcellations, we reasoned that a data-driven approach to hippocampal parcellation is necessary. To this end, we implemented a group masked independent components analysis to identify functional subunits of the hippocampus, most notably separating the anterior hippocampus into separate anterior-medial, anterior-lateral, and posteroanterior-lateral components. Measuring IVS across these components revealed a decrease in IVS along the medial-lateral axis of the anterior hippocampus but an increase from anterior to posterior. We conclude that intervoxel similarity is deeply affected by parcellation and that grounding one's parcellation in a functionally informed approach might allow for a more complex and reliable characterization of the hippocampus.

Key words: **anteroposterior; granularity; hippocampus; intervoxel similarity; long axis; uncus**

Significance Statement

Processing information along hierarchical scales of granularity is critical for many of the feats of cognition considered most human. Recently, the changes in structure, cortical connectivity, and apparent functional properties across parcels of the hippocampal long axis have been hypothesized to underlie this hierarchical gradient in information processing. We show here, however, that the choice of parcellation method itself drastically affects one particular measure of granularity across the hippocampus and that a functionally informed approach to parcellation reveals gradients both within the anterior hippocampus and in nonlinear form across the long axis. These results point to the issue of parcellation as a critical one in the study of the hippocampus and reorient interpretation of existing results.

Introduction

It is a key challenge for our memory system to extract and store general knowledge of the world while simultaneously retaining details of the individual episodes that make it up. For example, after seeing a number of shows at the jazz club downtown, one is able to call on generalized representations to predict what the next set will be like and identify similar music on the radio, all while being able to precisely reconstruct where one sat during a particular performance on a rainy night 2 years ago. Previous work has proposed that the processing of information at these hierarchical levels of detail may be dependent on distinct functional specializations along the long axis of the hippocampus (Poppenk et al., 2013; Strange et al. 2014; Sekeres et al., 2018). Specifically, it has been argued that hippocampal representations become increasingly finer grained along the long axis, with integrative, coarse-grained

Received Feb. 1, 2022; revised Aug. 9, 2022; accepted Aug. 12, 2022.

Author contributions: J.N.T. and L.D. designed research; J.N.T. performed research; C.G. and E.B. contributed unpublished reagents/analytic tools; J.N.T. analyzed data; and J.N.T. and L.D. wrote the paper.

This work was supported by National Institutes of Health–National Institute of Mental Health Grant R01-MH-076492 to L.D. We thank Catalina Yang for refining a color palette suitable for the study of the long axis.

The authors declare no competing financial interests.

Correspondence should be addressed to Lila Davachi at ld24@columbia.edu.

https://doi.org/10.1523/JNEUROSCI.0269-22.2022

representations in the anterior end and differentiated, fine-grained representations in the posterior end.

As a direct test of this proposed gradient, Brunec et al. (2018) measured the average temporal correlation across voxels, termed intervoxel similarity (IVS), as a putative index of the granularity of hippocampal information processing. Mathematically, IVS is the mean correlation between BOLD activity time courses of all voxels within a given region of interest (Fig. 1*A*). Lower IVS values therefore indicate that the temporal activation profiles in voxels within a particular anatomic region are relatively uncoupled from each other, which has been taken to reflect more distinct information processing in adjacent voxels and therefore greater representational granularity. Using this measure, Brunec et al. (2018) reported that during virtual navigation as well as during rest, the anterior hippocampus displayed higher IVS than the posterior hippocampus, suggesting that the anterior hippocampus may support representations that are intrinsically coarser-grained than in its posterior counterpart.

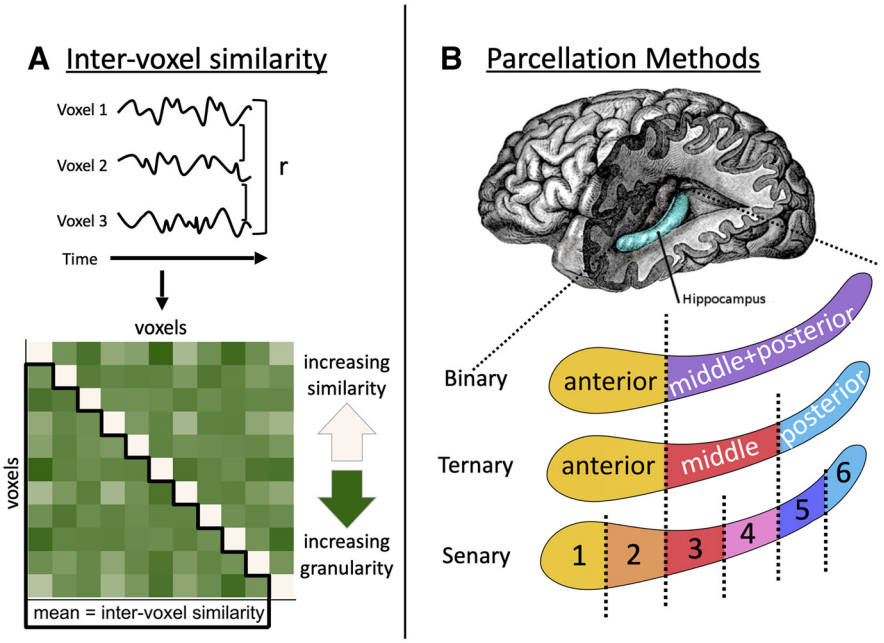

Figure 1. Overview of methods. ***A***, Diagram of IVS, the mean pairwise correlation of the entire time series of every voxel within a given parcel of the hippocampus. Decreases in IVS are taken as indications of individual voxels being sensitive to more distinct information and therefore processing representations with a higher granularity. ***B***, Proportional parcellations split the hippocampus (top) at roughly the uncal apex (binary parcellation), into even thirds (ternary parcellation), or into even sixths (senary parcellation).

Interestingly, other applications of IVS along the long axis have found inconsistent results in both developmental (Callaghan et al., 2021) and healthy aging (Stark, 2021) samples, namely, that IVS in these populations increases from anterior to posterior hippocampus. A major roadblock in reconciling findings across the long axis, however, is the variation in parcellation methods used to divide the hippocampus into its constituent subregions. Researchers have most typically divided the hippocampal long axis into binary, ternary, and senary (Fig. 1*B*) parcellation methods, the former two of which fall in line with structural and genetic transitions, respectively (Poppenk et al., 2013; Strange et al., 2014). Although much of the literature has assumed the choice of parcellation method to be relatively trivial, a thorough understanding of its impact is critical to proper interpretation of functional measures like IVS.

In the current study, we first used a large resting-state sample across two fMRI acquisition sequences (Acquisition 1, $N = 233$; Acquisition 2, $N = 176$) to compare the pattern of IVS across the hippocampus when using canonical parcellation methods (i.e., binary, ternary, senary). Although we should expect these proportional parcels to provide a rough summary of the differences across the long axis, it is unlikely to be the case that they have perfectly localized the natural joints of the emergent functional subunits we aim to study. Therefore, we adopted an additional analytical approach in which we applied group masked independent components analysis (mICA) to the resting-state signals in the hippocampus, which essentially identifies the spatial map that maximizes the statistical independence across individual components (Blessing et al., 2016; Moher Alsady et al., 2016; Blessing et al., 2020). We then compared IVS across these functionally derived parcels, stepping closer to a true characterization of functional gradients across the hippocampus.

Materials and Methods

fMRI dataset

Analyses were performed on the Nathan Kline Institute Rockland Sample, a lifespan cross-sectional dataset obtained at the Nathan Kline Institute and made publicly available online (Nooner et al., 2012). Participants were scanned on a SIEMENS 3T MRI scanner. A high-resolution 3D MPRAGE T1-weighted anatomic (TR = 1900 ms, voxel size = 1 mm isotropic, FOV = 250 mm) was first obtained, followed by two separate resting-state scans with differing acquisition parameters. The first resting-state scan (TR = 2500 ms, TE = 30 ms, voxel size = 3 mm × 3 mm × 3.5 mm, duration = 5 min, FOV = 216 mm) is referred to as Acquisition 1, and the second resting state scan (TR = 1400 ms, TE = 30 ms, voxel size = 2 mm isotropic, duration = 10 min, FOV = 216 mm, multiband acceleration factor 4) referred to as Acquisition 2 (Table 1). Participants were only instructed to keep their eyes open and fixate on the screen for the duration of each scan.

fMRI preprocessing

The fMRI preprocessing steps we applied are in line with the pipeline used by Brunec et al. (2018), with the exception that Statistical Parametric Mapping 12 (SPM12) was used rather than SPM8. In Acquisition 1, functional images were slice-time corrected, realigned, and resliced in accordance with the mean functional image, and coregistered to the space of the anatomic images. Acquisition 2 was preprocessed identically except that slice-time correction was not performed because of its faster TR during multiband acquisition. The anatomic images were then segmented into CSF and white matter (WM) images, which were thresholded at 0.7 and 0.9 (Qing et al., 2015), respectively, and eroded. These masks were used to extract CSF and WM time series from the functional images. The six motion regressors extracted from realignment as well as the CSF and WM time series were then entered as multiple regressors in a denoising generalized linear model (GLM).

Conservative motion and BOLD interpolation

The residuals of this GLM (the denoised functional timeseries) were then fed through a data interpolation method based on principal

Table 1. Scan acquisition parameters across studies

Acquisition	TR (ms)	TE (ms)	Voxel size (mm)	Duration (min)	FOV
Brunec et al. (2018)	2000	24	3.5 × 3.5 × 3.5	6	20 cm^2
Acquisition 1	2500	30	3 × 3 × 3.5	5	216 mm
Acquisition 2	1400	30	2 × 2 × 2	10	216 mm

Acquisition 1 more closely aligns with the scan parameters used during the resting-state analysis in Brunec et al. (2018).

components analysis (PCA; Campbell, 2013; Brunec et al., 2018). Because our analysis of the heterogeneity of individual voxel time series is sensitive to overly liberal interpolation, the method employed here only interpolates a time point if both its motion regressors and BOLD signal are significantly far from their own medians (Campbell et al., 2013). First, PCAs were run on both the matrix of six motion regressors over time and the matrix of voxel activity over time. Then, for each time point, the squared, normalized distance between the time point and the median of the surrounding 15 time points was calculated, resulting in a vector of distances from the median for each time point for each matrix. A gamma distribution was then estimated for each vector, and the cumulative density function estimated for each time point. Time points that had a $p < 0.05$ in both the six motion regressors and the functional time series were interpolated using spline interpolation. In other words, only time points that were significant outliers in both their overall motion and BOLD signal were removed and interpolated using surrounding data points.

Proportional parcellations

To define a mask for each participant's hippocampus, anatomic images were segmented into subcortical structures using the recon-all function in FreeSurfer (version 7.1.1; Fischl, 2012). These subcortical atlases were then transformed back into native space, and the bilateral hippocampus masks were extracted.

To mirror hippocampal parcellation approaches adopted by previous studies, we divided the hippocampus into subregions along the long axis by following three separate parcellation methods. For our binary parcellation, the hippocampus was divided into an anterior third and a combined two-thirds of middle-plus-posterior (Fig. 1*B*, left). This parcellation serves to approximate that used by Brunec et al. (2018), who split the individual hippocampi at the uncal apex into anterior and posterior parcels, and is similar to previous specifications (Poppenk et al., 2013; Brunec et al., 2020). For our ternary parcellation, we divided the hippocampus into even anterior, middle, and posterior thirds along the long axis (Collin, 2015; Tompary and Davachi, 2017; Dandolo and Schwabe, 2018; Callaghan et al., 2021). Finally, we also split the hippocampus into even sixths in a senary parcellation (Stark et al., 2021).

Masked group independent components analysis

Although the proportional parcellations described above might offer a rough approximation of unidimensional changes in granularity across the long axis, they also rest on top-down assumptions about how to identify meaningful hippocampal subunits. As such, also sought to parcellate the hippocampus based on the observed structure of activity within its constituent voxels (i.e., in a data-driven manner). Scans from 183 participants (for Acquisition 2) were submitted to an mICA using Functional MRI of the Brain Software Library (FSL) Multivariate Exploratory Linear Optimized Decomposition into Independent Components (MELODIC) implemented with the mICA toolbox (version 1.18). In the masked group ICA, a dimensionality of 10 was chosen based on previous research showing that 10 components display the highest split-half reproducibility without overparcellating the hippocampus (Blessing et al., 2016).

Extended fMRI preprocessing for group mICA

Because of multiband slicing artifacts present in Acquisition 2, data were first cleaned using the FIX FSL package (version 1.06; Griffanti et al., 2014; Salimi-Khorshidi et al., 2014). The FIX FSL package essentially functions by isolating individual components intrinsic to the data using MELODIC ICA, classifying components as noise or signal, and regressing noise components out of the data. We specifically implemented the training dataset WhII_MB6 that comes with the FIX FSL package, which closely aligned with the scan parameters from Acquisition 2 and used the default threshold of 20% confidence to binarize signal from noise. These cleaned functional images were only used for creating the group parcellation, and IVS was still calculated using the original images.

The functional images cleaned using the FIX FSL package were then smoothed using a smoothing kernel with a full-width half-maximum of 6 mm. A high-pass filter was then applied to the functional images with a cutoff of 100 s. Functional images from all participants were then normalized to the MNI avg152 T1-weighted template (2 mm isotropic resolution).

Group masked ICA parcellation

We then implemented the group masked ICA, which concatenated all 183 functional images (from Acquisition 2) and masked them with the Harvard-Oxford bilateral hippocampal mask thresholded at 50%, as in previous studies (Blessing et al., 2016, 2020; Moher Alsady et al., 2016). MELODIC ICA, with a dimensionality of 10, was then performed as previously described. Briefly, the data were demeaned and normalized by the voxelwise variance, projected into a 10-dimensional space using probabilistic PCA, and decomposed into spatial maps and time series using a fixed-point iteration technique optimizing for non-Gaussian spatial distribution. The resulting group-level spatial maps of each component were then divided by the SD of the residual noise and thresholded with a mixture model fitted to the histogram of each component to yield a *z*-transformed spatial map for each component. This process therefore yields the spatial maps of 10 functionally derived parcels of the hippocampus.

Warping group masked ICA parcels into native space

To use these spatial maps as individual masks for parcellating the hippocampus, each component was manually labeled based on the five locations within the hippocampus, thresholded at 0.5, and binarized. As the components from the ICA are not necessarily spatially cohesive (i.e., they are not constrained to one contiguous region), all voxels that were not spatially contiguous with the area containing the maximum *z* score were erased using the FreeView edit function. The component masks were then warped back into native space. To better align the components with the hippocampus in native space, the full Harvard-Oxford hippocampus mask was also warped into each participant's native space and linearly coregistered with the FreeSurfer hippocampal mask used before. The registration matrix retrieved from this step was then applied to each of the components, ensuring that each component was as closely aligned to its true location in native space as possible.

To confirm that the components derived from the mICA were indeed aligned properly within the FreeSurfer hippocampal mask, we calculated the proportion of the component mask that overlapped with the FreeSurfer mask for each participant and component. Any participant's component not overlapping at least 70% with the FreeSurfer mask was excluded from further analyses, although results were qualitatively similar without this exclusion.

Extracting parcel time series

Voxelwise time series were then extracted from the functional image using the hippocampal masks. This procedure produced a single time series for each voxel, scan, and participant in each of our hippocampal parcels.

Controlling for parcel size and shape

To control for the variable sizes and shapes of the parcels, the average distances between the location of each voxel and the center voxel were calculated separately for each of the *x*, *y*, and *z* axes within each parcel, acquisition, and participant as performed in Brunec et al. (2018). These average distances were then converted into units of millimeters along each dimension and later entered as parcel-level covariates in subsequent mixed effects models.

Intervoxel similarity calculation and exclusion criteria

All time series analyses were conducted using R (version 3.5.0) and RStudio software. A correlation matrix for each participant, hemisphere, and hippocampal parcel was constructed by first *z*-scoring the time series within each voxel, and then finding the correlation of the time series of each voxel with the time series of every other voxel within a given mask. Using original code from Brunec et al. (2018), the resulting correlation matrices were then Fisher *z*-transformed, the diagonal and upper triangle removed, and the mean of the resulting vector computed. This procedure resulted in one value of IVS per hippocampal parcel, acquisition, and participant. To protect against signal dropout, any hippocampal parcel missing data from >30% of voxels was also excluded.

Only scans with >0.55 mm mean frame displacement were excluded from the analysis (Satterthwaite et al., 2012). Because of a coding error, the mICA was performed using scans with <0.56 mm mean frame displacement, so six subjects whose mean frame displacement fell between 0.55 and 0.56 were included in the mICA parcellation but excluded from the final analysis. Our mICA parcellation visually replicates previous iterations, and including these subjects in the analysis does not change the results.

Finally, individual outlier values of IVS were excluded by first grouping values by acquisition, hemisphere, and parcel. Values that were farther than 1.5 times the interquartile range of this distribution from its median were assumed to be because of scanner noise and excluded from further analyses. This left $N = 233$ participants (116 females, 1 undisclosed, mean age 24.96, SD = 4.46) in Acquisition 1, and $N = 176$ participants (82 females, mean age 25.14, SD = 4.54) in Acquisition 2.

Statistical analyses

Mixed effects models predicting intervoxel similarity. Linear mixed effects models were performed using the lmer() function from the lme4 package (Bates et al., 2015) in R. Separate models were run per acquisition. For models used to compare ternary and binary parcellation methods, IVS was entered as the dependent variable; hemisphere (effect coded left, −0.5; right, 0.5), parcel (anterior, middle, middle-plus-posterior, posterior; reference, anterior), and their interactions were entered as independent variables. Models accounting for parcel size and shape included *x*_mean_distance, *y*_mean_distance, and z_mean_distance as covariates (see above, Controlling for parcel size and shape). All models included a random intercept grouped by participant, as was done in Brunec et al. (2018).

For our senary parcellation of even sixths, one model was used to extract the parcelwise confidence intervals (SE), and another was used to find the slope and corresponding non-linear confidence intervals (see Fig. 4). Note that the parcelwise confidence intervals are only presented for visual purposes, and all statistical analysis are performed on the confidence intervals of the non-linear slopes. The first model was identical to those described above, except for the inclusion of six rather than four levels within the parcel variable (one, two, three, four, five, six; reference, one). Mean distances along the *x*, *y*, and *z* axes were included as covariates.

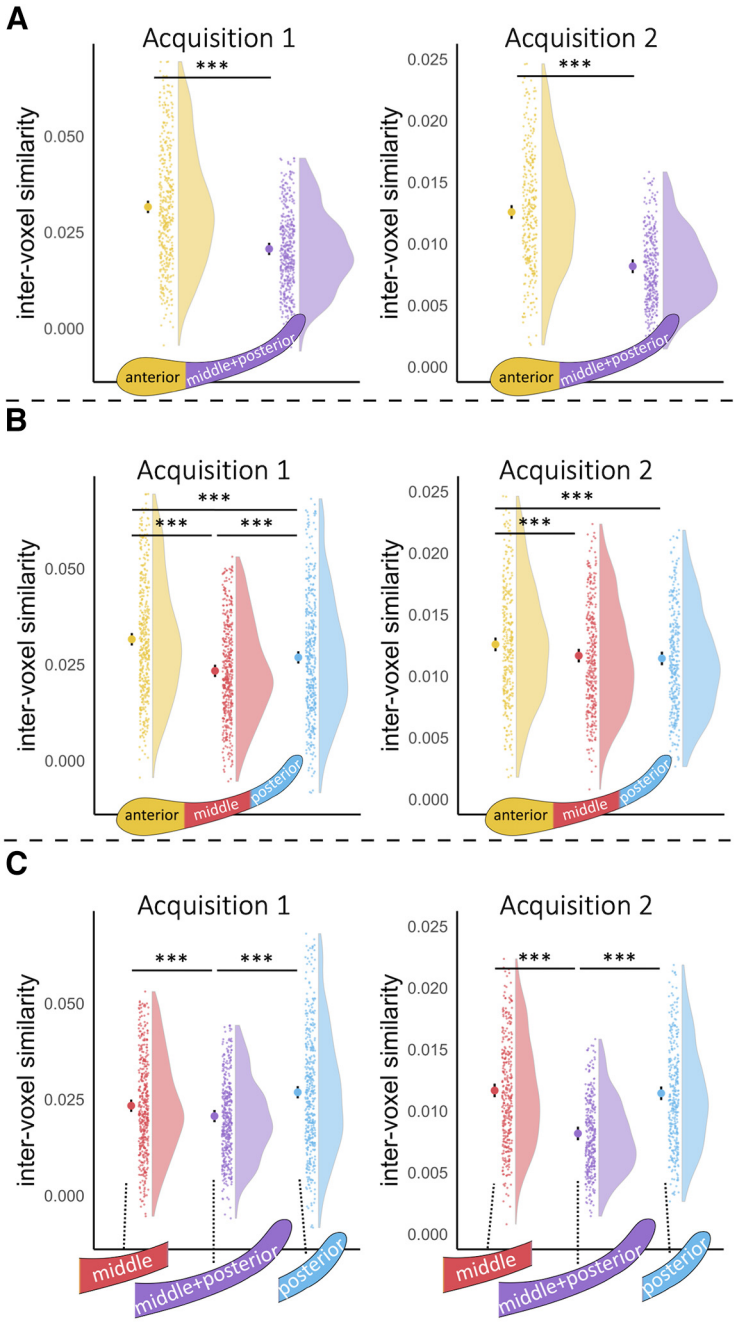

Figure 2. Binary parcellation underestimates the intervoxel similarity of the middle and posterior subregions. ***A***, In line with Brunec et al. (2018), we find that similarity within the anterior parcel (yellow) is higher than that in the middle-plus-posterior parcel (purple) across both acquisitions. ***B***, After splitting the middle-plus-posterior parcel into its constituent middle (red) and posterior (blue) parcels, as has been done previously, IVS seemed to be higher within the anterior parcel than that in the posterior parcel across both acquisitions. Although, interestingly, IVS within the middle parcel was lower than that in both the anterior and posterior parcels in Acquisition 1, in conflict with a linear decrease along the long axis. ***C***, Critically, however, the middle-plus-posterior parcel displayed a significantly lower IVS than both its constituent middle and posterior regions across both acquisitions, suggesting that combining these subregions into one misrepresents their apparent granularity. This last finding motivated our following analyses, which take the overall parcel size and shape into account. Error bars represent 95% confidence intervals. $^{***}p_{tukey} < 0.001$.

The linear model used to calculate the slope of the line of best fit along these parcels was the same as the one above except that the parcel factors were converted to their quantitative equivalents (1, 2, 3, 4, 5, 6, respectively) and were mean centered. Again, mean distances along the *x*, *y*, and *z* axes were included as covariates. We also ran a quadratic model that was the same as the linear model above except that it included a squared axis term. We compared the linear and quadratic models by

likelihood ratio chi-square test to select the best fitting models. The quadratic models provided a better fit to the data during both Acquisition 1 [$X^2(2) = 9.52$, $p = 0.009$] and Acquisition 2 [$X^2(2) = 12.11$, $p = 0.002$], so we therefore only report statistics from these quadratic models. To estimate p values for the calculated slopes, degrees of freedom were approximated for each fixed effect using the same Kenward–Roger method as for the estimated marginal means above.

The final mixed effects model was used to examine how IVS changed between the components derived from the mICA and was the same as the others above except for the factors within the parcel variable (anterior-medial, anterior-lateral, posteroanterior-lateral, middle, posterior; reference, anterior-medial). Again, mean distance along the x, y, and z axes were entered as covariates.

To directly compare IVS values across hippocampal parcels within hemisphere, the emmeans() function (https://CRAN.R-project.org/package=emmeans) in R was used to extract estimated marginal means for each parcel averaged across hemisphere from each model as well as to run pairwise t tests between parcels. Degrees of freedom were approximated using the Kenward–Roger method (Kenward and Roger, 1997), and p values were adjusted via Tukey's method for comparing a family of estimates of the given size (Tukey, 1949).

Data availability

Code for analyzing IVS and recreating figures is accessible at https://github.com/jnthorp/ivs-parcels_open.

Results

Our first goal was to investigate how IVS changes along the long axis of the hippocampus while specifically considering how these results differ across the multiple hippocampal parcellation methods often adopted by researchers in this field. We began by comparing IVS across binary (anterior vs middle-plus-posterior) and ternary (anterior vs middle vs posterior) parcellations, performing linear mixed effects regressions with a random intercept per participant, mirroring the primary analysis from Brunec et al. (2018). To directly compare IVS across hippocampal parcels, pairwise t tests were run between estimated marginal means of IVS computed for each parcel averaged across hemisphere. The Tukey method was used to correct for multiple comparisons within a family of four estimates (anterior, middle, middle-plus-posterior, and posterior). Separate mixed effects models were run for Acquisition 1 and Acquisition 2. Note that Acquisition 1 more closely aligns with the scan parameters implemented in Brunec et al. (2018), whereas Acquisition 2 provides many more voxels, TRs, and overall time points within each participant (Table 1).

Intervoxel similarity decreases from anterior to posterior hippocampus

We first aimed to replicate Brunec et al. (2018) by directly comparing IVS within the anterior parcel (yellow) to that in the middle plus posterior parcel (purple) across acquisitions (Fig. 2*A*). We found that IVS within the anterior parcel was significantly higher than that in the middle-plus-posterior parcel during both Acquisition 1 ($t_{(1428)} = 14.95$, $p_{tukey} < 0.001$) and Acquisition 2 ($t_{(1119)} = 18.89$, $p_{tukey} < 0.001$), which indeed mirrors the pattern observed during both resting-state and spatial navigation in Brunec et al. (2018).

Next, we computed IVS within ternary parcels (Collin et al., 2015; Dandolo and Schwabe, 2018; Callaghan et al., 2021) by splitting the middle-plus-posterior parcel into its constituent parts [middle (red) and posterior (blue) subregions]. As would be predicted by the prior result, IVS within the anterior third parcel remained higher than that in the posterior third parcel during Acquisition 1 ($t_{(1429)} = 6.47$, $p_{tukey} < 0.001$) as well as Acquisition 2 ($t_{(1119)} = 4.88$, $p_{tukey} < 0.001$; Fig. 2*B*).

Table 2. Influence of model covariates on intervoxel similarity

Acquisition	Parcellation	Covariate	*B*	SE	*t*
1	Ternary/binary	Hemisphere	0.0021	0.0010	2.06
		x	−0.0019	0.0008	−2.31
		y	0.0003	0.0006	0.59
		z	−0.0021	0.0007	−3.13
	Senary	Hemisphere	0.0029	0.0010	3.01
		x	−0.0004	0.0008	−0.50
		y	−0.0005	0.0008	−0.62
		z	−0.0023	0.0009	−2.42
2	Ternary/binary	Hemisphere	0.0007	0.0003	2.15
		x	−0.0007	0.0003	−2.39
		y	−0.0002	0.0003	−0.83
		z	−0.0013	0.0003	−5.37
	Senary	Hemisphere	0.00061	0.0003	2.39
		x	−0.0007	0.0003	−2.96
		y	−0.0012	0.0007	−1.79
		z	−0.0026	0.0003	−8.28
	mICA	*x*	−0.0025	0.0007	−3.60
		y	−0.0005	0.0005	−1.02
		z	−0.0036	0.0006	−6.28

Acquisition is as defined in Table 1. All models predicted intervoxel similarity with fixed effects of hemisphere (effect coded), parcel, their interactions, three covariates corresponding to the average distance between each voxel and the middle voxel along the *x*, *y*, and *z* axes, and a random intercept per subject. Ternary/binary parcellation models compared intervoxel similarity between the anterior, middle, middle-plus-posterior, and posterior parcels. Senary models compared intervoxel similarity across parcels of even sixths. mICA compared intervoxel similarity across functionally derived components. *B*, Unstandardized beta values. As the R function lmer() purposefully doesn't calculate degrees of freedom within each regressor, *t* values are shown without corresponding *p* values. SE, standard errors.

U-shaped change in intervoxel similarity along ternary parcels

Prior work examining the hippocampus with this ternary approach has most typically provided evidence that the middle hippocampus appears as a linear combination of what is seen in the anterior and posterior hippocampus (Collin et al., 2015; Dandolo and Schwabe, 2018; Callaghan et al., 2021). Thus, one strong prediction might be that IVS should smoothly decrease from anterior to middle to posterior hippocampus. Following this prediction, we found that IVS within the anterior parcel was significantly higher than that in the middle parcel during Acquisition 1 ($t_{(1425)} = 11.27$, $p_{tukey} < 0.001$) as well as Acquisition 2 ($t_{(1117)} = 3.93$, $p_{tukey} < 0.001$; Fig. 2*B*). However, in contrast to what would have been predicted by a linear gradient in granularity, IVS within the middle parcel was also lower than that in the posterior parcel during Acquisition 1 ($t_{(1419)} = -4.90$, $p_{tukey} < 0.001$), although not during Acquisition 2 ($t_{(1114)} = 0.98$ $p_{tukey} = 0.76$).

The middle-plus-posterior parcel exaggerates the granularity of its constituent subregions

To further unravel the systematic differences between these binary and ternary parcels, we next considered the relationship between the apparent granularity measured within the combined middle-plus-posterior parcel and that of its constituent middle and posterior parcels (when calculated separately). We found that the middle-plus-posterior parcel consistently displayed lower IVS than that in the middle parcel during both Acquisition 1 ($t_{(1414)} = -3.78$, $p_{tukey} < 0.001$) and Acquisition 2 ($t_{(1113)} = -15.20$, $p_{tukey} < 0.001$) as well as the posterior parcel during both Acquisition 1 ($t_{(1416)} = -8.70$, $p_{tukey} < 0.001$) and Acquisition 2 ($t_{(1112)} = -14.21$, $p_{tukey} < 0.001$; Fig. 1*C*).

This pattern of results suggests that combining these potentially distinct subregions into the same parcel and correlating their voxel time series together may artificially lower the apparent IVS within the unified parcel. In other words, it may be that the low IVS within the middle-plus-posterior region is more directly caused by the mixing of disparate signals from middle and posterior hippocampus rather than the individual voxels in this subregion being relatively uncoupled from each other. Not only does this overaccentuate the difference in granularity between the anterior and posterior subregions, it also glosses over what may be a more complex U-shaped gradient in processing from anterior to middle to posterior hippocampus.

Accounting for parcel size and shape accentuates U-shaped change in ternary parcels

One way to account for the overestimation of the middle-plus-posterior parcel of its own granularity is to add control variables for the overall size and shape of each parcel. Because we would expect the time series of voxels anatomically farther away from one another to be less similar to each other, a parcel that spans a longer distance along the hippocampus may display a lower IVS simply by nature of including voxels anatomically farther apart. Thus, we implemented a control analysis from Brunec et al. (2018), which simply adds covariates to each model to account for the spatial size of each parcel along the *x*, *y*, and *z* axes. Unstandardized betas for each covariate are reported in Table 2. The resulting model estimates therefore more precisely represent the decoupling of individual voxel time series from one another, controlling for the average anatomic distance between them.

Although IVS in the anterior parcel remained higher than that in the middle-plus-posterior parcel during Acquisition 1 ($t_{(1521)} = 4.29$, $p_{tukey} < 0.001$), consistent with Brunec et al. (2018), this difference was not statistically significant during Acquisition 2 ($t_{(1213)} = 1.39$, $p_{tukey} = 0.50$; Fig. 3*A*). Similarly within our ternary parcels, although IVS in the anterior parcel remained higher than that in the posterior parcel during Acquisition 1 ($t_{(1551)} = 3.87$, $p_{tukey} < 0.001$), this difference was again not statistically significant during Acquisition 2 ($t_{(1213)} = 1.67$, $p_{tukey} = 0.34$; Fig. 3*B*). Across both parcellation methods, therefore, apparent

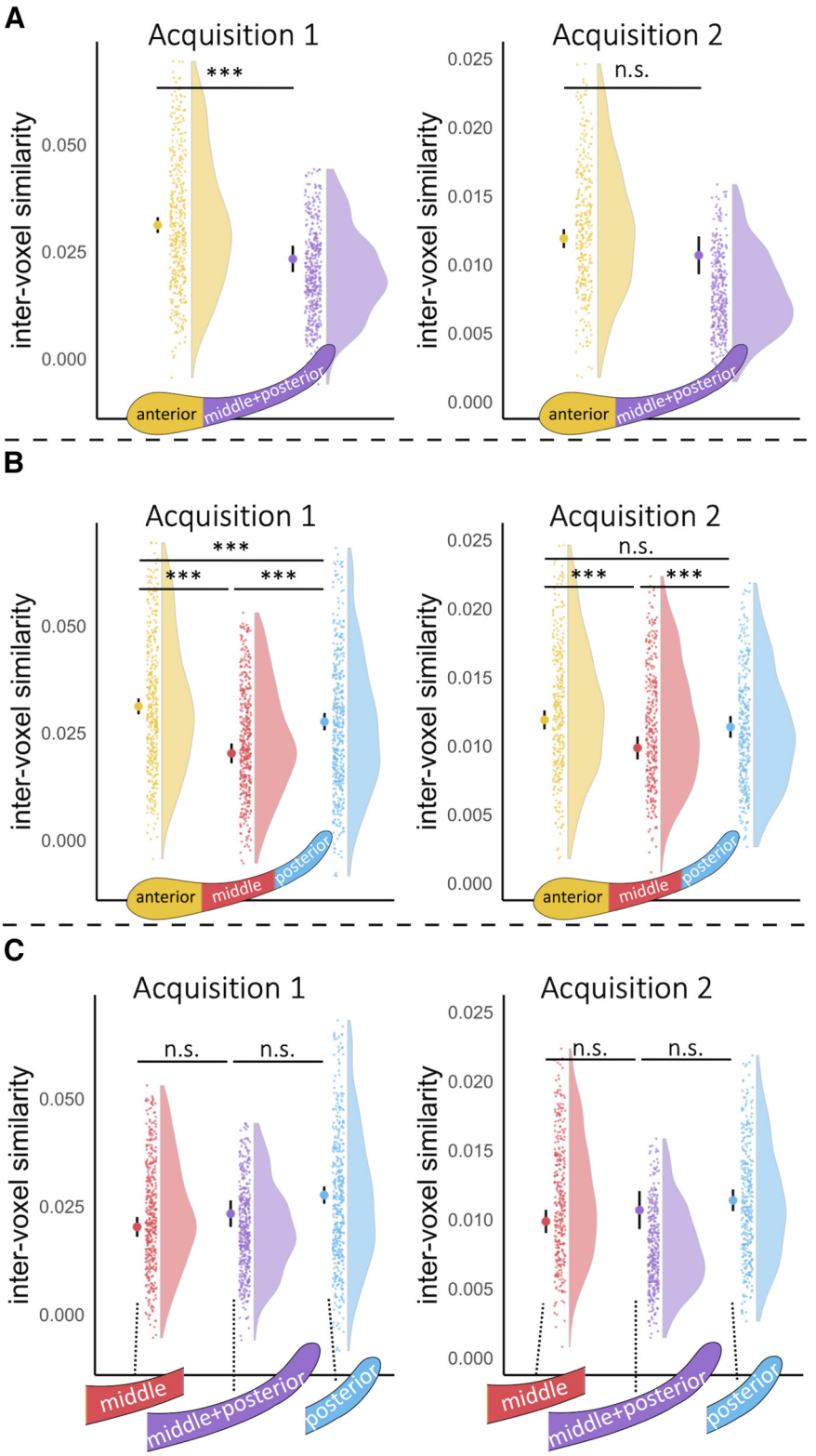

Figure 3. Controlling for parcel size and shape reinforces a U-shaped change in granularity along the long axis. To account for the discrepancies in length, width, and height among the different parcels, covariates for parcel size and shape were added to the models, as was accounted for in a later analysis in Brunec et al. (2018). ***A***, After entering these covariates, we still found substantial evidence for the original comparison between anterior and middle-plus-posterior in Acquisition 1, but not in Acquisition 2. ***B***, In our ternary parcels, the anterior parcel displayed a higher IVS than that in the posterior parcel in Acquisition 1, but not in Acquisition 2. Across both acquisitions, however, IVS in the middle parcel was lower than that in both the anterior and posterior parcels, reinforcing the U-shaped change along the long axis. ***C***, As was the intended result of adding these covariates, no differences were found between the middle-plus-posterior parcel and its constituent middle and posterior parcels, as these were completely accounted for by their differences in size and shape. Error bars represent 95% confidence intervals. ***$p_{tukey} < 0.001$. n.s. not significant.

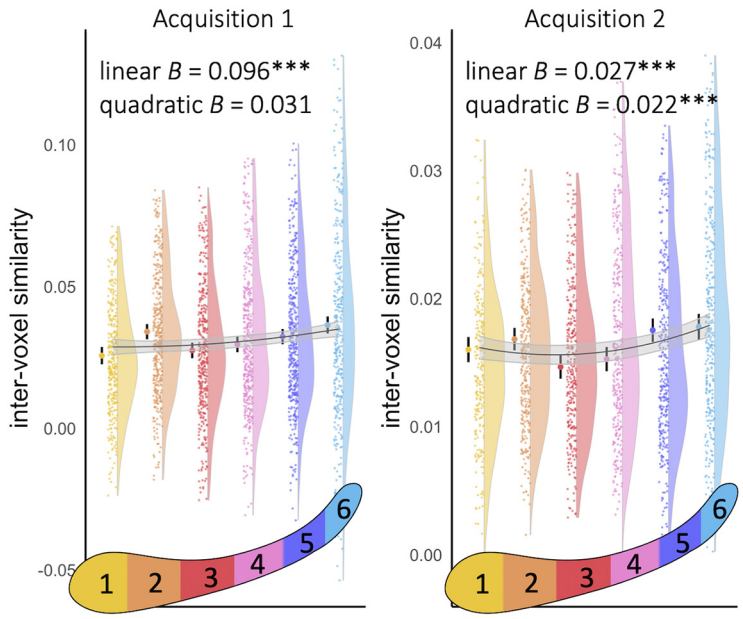

Figure 4. Intervoxel similarity increases across parcels of even sixths. When modeled linearly, intervoxel similarity shows a significant increase from anterior to posterior across parcels of even sixths in both acquisitions. Error bars are 95% confidence intervals within each parcel. Black lines indicate the estimated non-linear relationship. Gray ribbons represent 95% confidence intervals from non-linear model. *** $p < 0.001$.

differences in granularity between anterior and posterior hippocampus are left intact during Acquisition 1 but are well accounted for by parcel size and shape during Acquisition 2.

In contrast, the addition of these parcel size and shape covariates only served to strengthen the U-shaped change in IVS from anterior to middle to posterior hippocampus. That is, IVS in the middle parcel remained lower than that in the anterior parcel in both Acquisition 1 ($t_{(1564)} = -10.17$, $p_{tukey} < 0.001$) and Acquisition 2 ($t_{(1243)} = -5.60$, $p_{tukey} < 0.001$), as well as lower than that in the posterior parcel in both Acquisition 1 ($t_{(1594)} = -5.92$, $p_{tukey} < 0.001$) and Acquisition 2 ($t_{(1232)} = -3.41$, $p_{tukey} = 0.004$). As anticipated, the addition of these covariates also accounted for the differences between middle-plus-posterior and its constituent middle and posterior parcels (all p_{tukey} values > 0.12; Fig. 3*C*). Together, these results across acquisitions seem to suggest that accounting for parcel size and shape reinforces a U-shaped gradient in IVS along the hippocampal long axis.

Intervoxel similarity increases along senary parcels of even sixths

To follow up on these results at a finer resolution, we performed mixed effects linear regressions examining IVS across senary parcels of even sixths. As above, this model included fixed effect covariates of mean distance along the *x*, *y*, and *z* axes and a random intercept grouped by subject. Because we have just presented evidence of a U-shaped change from anterior to posterior, we also ran models that included a quadratic term across parcels interacting with hemisphere. We compared the linear and quadratic models by likelihood ratio chi-square test to select the best fitting models. The quadratic models provided a better fit to the data during both Acquisition 1 [$X^2(2) = 9.52$, $p = 0.009$] and Acquisition 2 [$X^2(2) = 12.11$, $p = 0.002$].

Directly conflicting with the findings in Stark et al. (2021) in young adults, we found evidence of a linear increase along the long axis (from anterior to posterior) in both Acquisition 1 ($B = 0.096$, $t_{(2179)} = 3.91$, $p < 0.001$) as well as Acquisition 2 ($B = 0.027$, $t_{(1746)} = 4.30$, $p < 0.001$). Although we did not find evidence of quadratic change along the long axis during Acquisition 1 ($B = 0.031$, $t_{(2093)} = 1.32$, $p = 0.19$), we found substantial evidence during Acquisition 2 ($B = 0.022$, $t_{(1757)} = 3.42$, $p < 0.001$). In other words, modeling IVS linearly and quadratically using this senary parcellation showed IVS to be highest (least granular) in posterior hippocampus, with a U-shaped change from anterior to posterior that was strongest in Acquisition 2. These inconsistent results across parcellation methods and acquisitions should suggest to us that slicing unilaterally across the hippocampus may not be carving at the most relevant joints. That is, just as the middle-plus-posterior parcel may combine signals across disparate middle and posterior subregions, it may be the case that any of our typical, proportional parcellation methods inadvertently combine data across disparate clusters of functional activity.

Group masked independent components analysis

Our results thus far demonstrate that the proportional parcellation techniques largely adopted by the field fall short of characterizing the true functional subunits of the hippocampus. As such, we next aimed to parcellate the hippocampus based on the underlying structure of the functional signals themselves. To this end, we ran a group mICA (Blessing et al., 2016, 2020; Moher Alsady et al., 2016) that effectively separates the hippocampus into the 10 components that maximize the spatial independence between components and the temporal coherence within components. Because of the comparatively higher number of TRs in Acquisition 2, only Acquisition 2 was submitted to the mICA and used in the following set of analyses, which benefit greatly from more within-subject data. This procedure resulted in the bilateral hippocampi being clustered into 10 distinct regions, five in each hemisphere, as follows: three splitting the anterior hippocampus (anterior-medial, red; anterior-lateral, yellow; posteroanterior-lateral, green), one in the middle hippocampus (light blue), and one in the posterior hippocampus (dark blue; see Fig. 5*A*). Split-half reproducibility analyses resulted in an average Pearson's correlation of 0.966 across components, showing that randomly splitting the sample into discrete halves had virtually no effect on the spatial layout of the components. Previous work has shown 10 components to maximize this split-half reproducibility correlation, with fewer than 10 components leaving large parts of the hippocampus unassigned to a particular component and >10 components unnecessarily splitting components into smaller, less reliable parcels (Blessing et al., 2016).

To gain a better understanding of how granularity, as measured by IVS, might differ across these functional subregions, we next calculated IVS within each component and ran a linear mixed effects model predicting IVS by hippocampal component and hemisphere. As above, this model included fixed effect covariates of mean distance along the *x*, *y*, and *z* axes and a random intercept grouped by subject. Because of the fact that the mICA creates slightly different parcels across hemispheres, we performed all *t* tests within hemisphere, implementing the Tukey method to correct for a family of five tests in each hemisphere.

mICA finds a medial-lateral gradient within anterior hippocampus

When looking at these functionally derived components, we again found evidence of a U-shaped gradient in IVS between the anterior-medial component (red) and the posterior component (blue; see Fig. 5*B*). IVS within the posterior parcel was higher than that in the anterior-medial component (red) in the left ($t_{(1314)}$ = 3.22, p_{tukey} = 0.011) but not right ($t_{(1344)}$ = 1.23, p_{tukey} = 0.73) hemisphere, anterior-lateral component (yellow) in the left ($t_{(1284)}$ = 5.92, p_{tukey} < 0.001) but not right ($t_{(1346)}$ = 2.32, p_{tukey} = 0.14) hemisphere, the posteroanterior-lateral component (green) in both the left ($t_{(1318)}$ = 7.42, p_{tukey} < 0.001) and right ($t_{(1317)}$ = 4.63, p_{tukey} < 0.001) hemispheres, as well as the middle component (light blue) in both the left ($t_{(1304)}$ = 7.63, p_{tukey} < 0.001) and right ($t_{(1338)}$ = 3.43, p_{tukey} = 0.005) hemispheres. IVS within the anterior-medial component (red) was then higher than that in the middle component in the left ($t_{(1270)}$ = 4.60, p_{tukey} < 0.001) and right ($t_{(1316)}$ = 2.87, p_{tukey} = 0.034) hemispheres.

Critically, we also found a decrease in IVS along the medial-lateral axis of the anterior hippocampus. That is, IVS within the anterior-medial component was higher than that in the posteroanterior-lateral component in both the left ($t_{(1281)}$ = 4.16, p_{tukey} < 0.001) and right ($t_{(1277)}$ = 3.89, p_{tukey} = 0.001) hemispheres, as well as than that in the anterior-lateral component in the left hemisphere ($t_{(1255)}$ = 2.87, p_{tukey} = 0.034), although this difference was not significant in the right hemisphere ($t_{(1364)}$ = 1.15, p_{tukey} = 0.78). These differences suggest what could be an important axis within the anterior hippocampus that has been left unexamined by typical proportional parcellation methods.

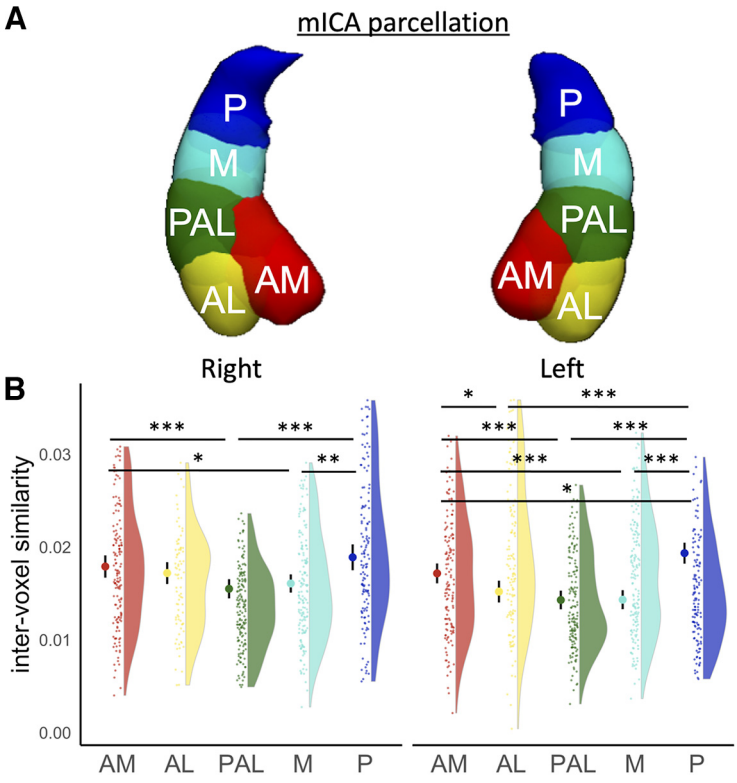

Figure 5. Data-driven parcellation of functional signals reveals a medial-lateral gradient of intervoxel similarity within the anterior hippocampus. ***A***, Parcellation as derived from group mICA. Replicating earlier work, the mICA split each hemisphere into anterior-medial (AM; red), anterior-lateral (AL; yellow), posteroanterior-lateral (PAL; green), middle, (M; light blue), and posterior (P; dark blue) components. ***B***, Because of differences in parcellation across hemispheres, we report differences in intervoxel similarity in both hemispheres. Contrary to our findings using proportional parcellations, intervoxel similarity was higher within the posterior parcel than that in the anterior-lateral, posteroanterior-lateral, and middle parcels across both hemispheres. Interestingly, intervoxel similarity within the anterior-medial parcel was higher than that in the middle, posteroanterior-lateral, and anterior-lateral parcel within the left hemisphere, and higher than that in the posteroanterior-lateral parcel in the right hemisphere. This suggests that processing granularity may differ along the medial-lateral axis within the anterior hippocampus, a difference that was inaccessible using the proportional parcellations used previously. Error bars represent 95% confidence intervals. *p_{tukey} < 0.05. **p_{tukey} < 0.01. ***p_{tukey} < 0.001.

Discussion

IVS is a measure of the statistical similarity of voxels within a given subregion, with decreasing similarity indicating greater informational capacity and therefore a finer grain of processing. In the context of episodic memory, the intuition is that subregions responsible for extracting features that overlap across episodes, objects, or larger temporal windows would contain voxels that were responsive to similar information and therefore were more temporally intertwined with one another. The degree of this temporal similarity has thus been used to suggest that intrinsic dynamics of information processing across the long axis of the hippocampus move from coarse-grained (high IVS) in the anterior to fine-grained (low IVS) in the posterior. Here, we used a large fMRI resting-state dataset to show that change in IVS along the long axis varies widely with the adopted parcellation method and seems to change along multiple gradients within the hippocampus.

We found that IVS decreases along binary hippocampal parcels from anterior to middle-plus-posterior (Fig. 6, Binary), in line with prior published reports. However, we also found that considering the middle and posterior thirds of the hippocampus as one middle-plus-posterior region artificially lowers the apparent IVS, ultimately suggesting that the IVS within this binary parcellation is not a reliable estimate of the true underlying signal variance. Accounting for the size and shape of the individual parcels then resulted in a U-shaped change in IVS along ternary parcels, with the middle parcel displaying lower IVS than that in the anterior and posterior parcels (Fig. 6, Ternary). A senary parcellation into even sixths further complicated the story, with IVS displaying a nonlinear increase from anterior to posterior hippocampus (Fig. 6, Senary), thereby suggesting the posterior hippocampus is actually coarser grained than its anterior counterparts as has been found in both developmental (Callaghan et al., 2021) and healthy aging (Stark et al., 2021) cohorts.

Thus, to take a step back, we came to the conclusion that parcellations drawn onto structural landmarks (i.e., the binary parcellation at the uncal apex) or genetic boundaries within the rodent hippocampus (i.e., the ternary parcellation) were not localizing the functional joints of the hippocampus. To more carefully localize these subunits before attempting to characterize them, we used a group mICA to identify hippocampal subregions that contain voxels with similar temporal coherence. This data-driven parcellation revealed subregions analogous

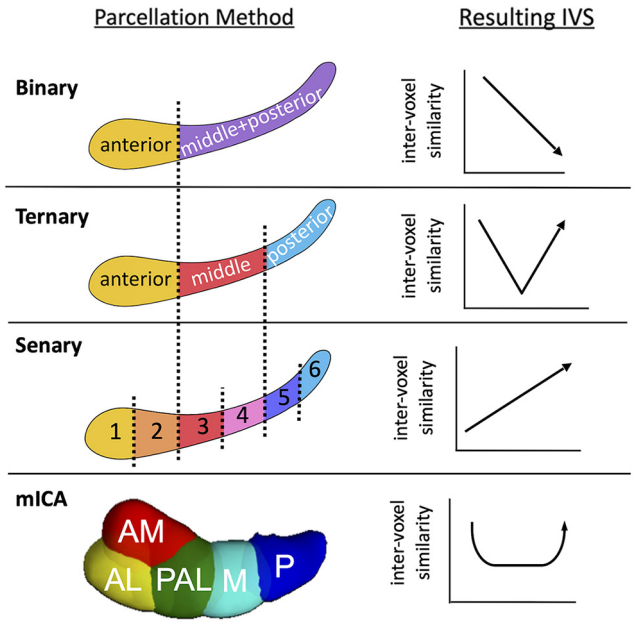

Figure 6. Summary of intervoxel similarity findings within all parcellation methods. Intervoxel similarity decreased along binary parcels, formed a U-shaped gradient along ternary parcels, increased along senary parcels of even sixths, and within the mICA parcellation both decreased along the medial-lateral axis within the anterior hippocampus and formed a U-shaped gradient from anterior-medial to posterior.

to those found across prior published studies (Blessing et al., 2016, 2020; Moher Alsady et al., 2016). Although this technique by definition will identify hippocampal clusters with relatively high levels of IVS, it is agnostic to differences in temporal coherence across distinct components, which is our measure of interest. Critically, this approach revealed a novel differentiation within the anterior hippocampus along its medial-lateral axis as well as U-shaped change from anterior to posterior, with IVS within the anterior-lateral and posteroanterior-lateral components lower than that in both the anterior-medial and posterior components (Fig. 6, mICA).

The principal takeaway from our findings, then, is simply that hippocampal IVS is deeply affected by parcellation. More generally, that carving the hippocampus in a manner unrelated to the underlying functional clustering fails to accurately represent its functional characteristics. Thus, it seems best to ground one's approach in a framework that doesn't rely on genetic or structural sign posts but rather the emergent organization of the functional signals themselves. Such approaches of identifying meaningful boundaries between regions of the brain have proved extremely successful in the realm of cortical network segmentation (Beckmann et al., 2005; Smitha et al., 2017; Bryce et al., 2021) but have yet to be the default method in intraregional parcellation. Of the concerted effort to parcellate the hippocampus in a data-driven manner (Zarei et al., 2013; Voets et al., 2014; Chase et al., 2015; Robinson et al., 2015; Wang et al., 2016; Barnett et al., 2019; Cheng et al., 2020), most of the resulting methods have relied on clustering second-order consequences of the voxel timeseries (e.g., the IVS matrices used here, hippocampo-cortical connectivity, univariate results across studies) and have often replicated the proportional parcellations already typical to the literature.

The mICA parcellation is therefore somewhat unique in dealing directly with the voxel activity time series themselves, repeatedly uncovering a medial-lateral distinction within the anterior hippocampus that seems to rest on the localization of the uncus within the anterior-medial component (Zeidman and Maguire, 2016). Crucially, the formation of the uncus, via the rostromedial inversion of the anterior hippocampus during embryonic development, is distinctive to primates in that the strict genetic demarcations found in the ventral hippocampus in rodents may not be representative of any such demarcations in the primate hippocampus (Strange et al., 2014). This medial-lateral distinction resonates with divergent findings where the anterior hippocampus may, at times, integrate overlapping item pairs during online concept formation (Davis et al., 2012a, b; Bowman and Zeithamova, 2018; Mack et al., 2018; Viganò and Piazza, 2021) or immediate memory retrieval (Ritchey et al., 2015; Libby et al., 2018), whereas, at other times, differentiate between specific items in memory (Tompary and Davachi, 2017; Ezzyat et al., 2018; Cowan et al., 2021). It may be that these distinct medial-lateral components help to resolve this conflict.

It's also worth noting the relatively consistent appearance of a U-shaped change in IVS from anterior to posterior, both across ternary parcels as well as our mICA components. Although we resist interpreting any of this too deeply without evidence of behavioral implications or validation of IVS across other measures, they raise an interesting question of whether it's appropriate to consider the middle hippocampus as simply a linear midpoint between the anterior and posterior hippocampus on our measures of interest (Collin et al., 2015; Dandolo and Schwabe, 2018; Callaghan et al., 2021). Future work is needed to explicitly probe the role of this functional unit of the hippocampus within the distributed memory system.

Limitations

IVS was first proposed to indicate more granular information processing that would underlie coding of specific contextual or visuospatial details in memory representations. The strongest interpretations of IVS have extended this measure to reflect the essential, intrinsic dynamics of the human hippocampus, ostensibly invariant to behavioral task demands or representational content. Adopting that logic here would extend our mICA parcellation results to be indicative of hippocampal processing generally, with greater integration in anterior-medial and posterior hippocampus and greater differentiation in anterior-lateral, posteroanterior-lateral, and middle hippocampus. Our varied results using proportional parcels, however, make clear that strong interpretations of IVS might be fragile to external factors. We therefore resist that level of interpretation here. That is, we do not necessarily predict that the patterns of IVS shown above are (1) stable features of the hippocampus that (2) hold the same computational role across every behavioral task, type of attended content, or motivational state the hippocampus might represent or be involved in.

It is therefore also important to note that we have only used one measure of spatiotemporal autocorrelation in this article, and thus it is important to consider that other measures may show stabler results across different parcellation methods. In previous work, IVS initially showed overlapping but nonequivalent results with the temporal autocorrelation measure also proposed in Brunec et al. (2018), particularly across smaller parcels in the posterior hippocampus during rest. In very recent work, Bouffard et al. (2021) showed that within-voxel temporal autocorrelation was highest in the anterior-medial hippocampus and lowest in the intermediate and posterior-lateral hippocampus. This convergence with our measures within the anterior-medial hippocampus suggests that this region should be considered distinct from the

anterior-lateral hippocampus in the focus of future work. The divergence between these two measures within the posterior hippocampus raises the intriguing possibility that voxels within the posterior hippocampus are relatively coherent with one another while exhibiting high variance from one TR to the next, a possibility that should only invite further inquiry into the characteristics and consequences of these separate measures rather than invalidate one in comparison to the other.

Because we do not hold ourselves to have uncovered an essential state of the hippocampus, we are reticent to draw strong functional conclusions from our resting-state findings. We are excited to pursue these questions in the context of fMRI tasks known to involve integration and differentiation within the hippocampus, but we are not prepared to make the same venture within a resting-state context. Future work should and will compare these intrinsic measures to trait- or state-level behaviors and, most importantly, examine how resting IVS is related to IVS during tasks when the hippocampus is engaged. By triangulating resting measures, behavior, and task responsive patterns in distinct hippocampal subregions, future work will be able to better understand how the hippocampal long axis represents and encodes experiences.

To us, then, the evidence here simply shows how sensitive neural measures are to one's prior organizational assumptions, and how complex and heterarchical the hippocampus can appear when those assumptions are abandoned.

References

Barnett AJ, Man V, McAndrews MP (2019) Parcellation of the hippocampus using resting functional connectivity in temporal lobe epilepsy. Front Neurol 10:920.

Bates D, Mächler M, Bolker B, Walker S (2015) Fitting linear mixed-effects models using lme4. J Stat Softw 67.

Beckmann CF, DeLuca M, Devlin JT, Smith SM (2005) Investigations into resting-state connectivity using independent component analysis. Philos Trans R Soc Lond B Biol Sci 360:1001–1013.

Blessing EM, Beissner F, Schumann A, Brünner F, Bär K-J (2016) A data-driven approach to mapping cortical and subcortical intrinsic functional connectivity along the longitudinal hippocampal axis. Hum Brain Mapp 37:462–476.

Blessing EM, Murty VP, Zeng B, Wang J, Davachi L, Goff DC (2020) Anterior hippocampal–cortical functional connectivity distinguishes antipsychotic naïve first-episode psychosis patients from controls and may predict response to second-generation antipsychotic treatment. Schizophrenia Bulletin 46:680–689.

Bouffard NR, Golestani A, Brunec IK, Bellana B, Barense MD, Moscovitch M (2021) Single voxel autocorrelation uncovers gradients of temporal dynamics in the hippocampus and entorhinal cortex during rest and navigation. bioRxiv 454036. doi:10.1101/2021.07.28.454036.

Bowman CR, Zeithamova D (2018) Abstract memory representations in the ventromedial prefrontal cortex and hippocampus support concept generalization. J Neurosci 38:2605–2614.

Brunec IK, Bellana B, Ozubko JD, Man V, Robin J, Liu Z-X, Grady C, Rosenbaum RS, Winocur G, Barense MD, Moscovitch M (2018) Multiple scales of representation along the hippocampal anteroposterior axis in humans. Curr Biol 28:2129–2135.e6.

Brunec IK, Robin J, Olsen RK, Moscovitch M, Barense MD (2020) Integration and differentiation of hippocampal memory traces. Neurosci Biobehav Rev 118:196–208.

Bryce NV, Flournoy JC, Guassi Moreira JF, Rosen ML, Sambook KA, Mair P, McLaughlin KA (2021) Brain parcellation selection: an overlooked decision point with meaningful effects on individual differences in resting-state functional connectivity. Neuroimage 243:118487.

Callaghan B, Gasser C, Silvers JA, VanTieghem M, Choy T, O'Sullivan K, Tompary A, Davachi L, Tottenham N (2021) Age-related increases in posterior hippocampal granularity are associated with remote detailed episodic memory in development. J Neurosci 41:1738–1754.

Campbell KL, Grigg O, Saverino C, Churchill N, Grady CL (2013) Age differences in the intrinsic functional connectivity of default network subsystems. Front Aging Neurosci 5:73.

Chase HW, Clos M, Dibble S, Fox P, Grace AA, Phillips ML, Eickhoff SB (2015) Evidence for an anterior–posterior differentiation in the human hippocampal formation revealed by meta-analytic parcellation of fMRI coordinate maps: focus on the subiculum. Neuroimage 113:44–60.

Cheng H, Zhu H, Zheng Q, Liu J, He G (2020) Functional parcellation of the hippocampus by semi-supervised clustering of resting state fMRI data. Sci Rep 10:16402.

Collin SHP, Milivojevic B, Doeller CF (2015) Memory hierarchies map onto the hippocampal long axis in humans. Nat Neurosci 18:1562–1564.

Cowan ET, Liu AA, Henin S, Kothare S, Devinsky O, Davachi L (2021) Time-dependent transformations of memory representations differ along the long axis of the hippocampus. Learn Mem 28:329–340.

Dandolo LC, Schwabe L (2018) Time-dependent memory transformation along the hippocampal anterior-posterior axis. Nat Commun 9:1205.

Davis T, Love BC, Preston AR (2012a) Learning the exception to the rule: model-based FMRI reveals specialized representations for surprising category members. Cereb Cortex 22:260–273.

Davis T, Love BC, Preston AR (2012b) Striatal and hippocampal entropy and recognition signals in category learning: simultaneous processes revealed by model-based fMRI. J Exp Psychol Learn Mem Cogn 38:821–839.

Ezzyat Y, Inhoff MC, Davachi L (2018) Differentiation of human medial prefrontal cortex activity underlies long-term resistance to forgetting in memory. J Neurosci 38:10244–10254.

Fischl B (2012) FreeSurfer. Neuroimage 62:774–781.

Griffanti L, Salimi-Khorshidi G, Beckmann CF, Auerbach EJ, Douaud G, Sexton CE, Zsoldos E, Ebmeier KP, Filippini N, Mackay CE, Moeller S, Xu J, Yacoub E, Baselli G, Ugurbil K, Miller KL, Smith SM (2014) ICA-based artefact removal and accelerated fMRI acquisition for improved resting state network imaging. Neuroimage 95:232–247.

Kenward MG, Roger JH (1997) Small sample inference for fixed effects from restricted maximum likelihood. Biometrics 53:983–997.

Libby LA, Reagh ZM, Bouffard NR, Ragland JD, Ranganath C (2018) The hippocampus generalizes across memories that share item and context information. J Cogn Neurosci 31:24–35.

Mack ML, Love BC, Preston AR (2018) Building concepts one episode at a time: the hippocampus and concept formation. Neurosci Lett 680:31–38.

Moher Alsady T, Blessing EM, Beissner F (2016) MICA-A toolbox for masked independent component analysis of fMRI data. Hum Brain Mapp 37:3544–3556.

Nooner KB, et al. (2012) The NKI-Rockland Sample: A Model for Accelerating the Pace of Discovery Science in Psychiatry. Front Neurosci 6:152.

Poppenk J, Evensmoen HR, Moscovitch M, Nadel L (2013) Long-axis specialization of the human hippocampus. Trends Cogn Sci 17:230–240.

Qing Z, Dong Z, Li S, Zang Y, Liu D (2015) Global signal regression has complex effects on regional homogeneity of resting state fMRI signal. Magnetic Resonance Imaging 33:1306–1313.

Ritchey M, Montchal ME, Yonelinas AP, Ranganath C (2015) Delay-dependent contributions of medial temporal lobe regions to episodic memory retrieval. Elife 4:e05025.

Robinson JL, Barron DS, Kirby LAJ, Bottenhorn KL, Hill AC, Murphy JE, Katz JS, Salibi N, Eickhoff SB, Fox PT (2015) Neurofunctional topography of the human hippocampus. Hum Brain Mapp 36:5018–5037.

Salimi-Khorshidi G, Douaud G, Beckmann CF, Glasser MF, Griffanti L, Smith SM (2014) Automatic denoising of functional MRI data: combining independent component analysis and hierarchical fusion of classifiers. Neuroimage 90:449–468.

Satterthwaite TD, Wolf DH, Loughead J, Ruparel K, Elliott MA, Hakonarson H, Gur RC, Gur RE (2012) Impact of in-scanner head motion on multiple measures of functional connectivity: relevance for studies of neurodevelopment in youth. Neuroimage 60:623–632.

Sekeres MJ, Winocur G, Moscovitch M (2018) The hippocampus and related neocortical structures in memory transformation. Neurosci Lett 680:39–53.

Smitha KA, Akhil Raja K, Arun KM, Rajesh PG, Thomas B, Kapilamoorthy TR, Kesavadas C (2017) Resting state fMRI: a review on methods in resting state connectivity analysis and resting state networks. Neuroradiol J 30:305–317.

Stark SM, Frithsen A, Stark CEL (2021) Age-related alterations in functional connectivity along the longitudinal axis of the hippocampus and its subfields. Hippocampus 31:11–27.

Strange BA, Witter MP, Lein ES, Moser EI (2014) Functional organization of the hippocampal longitudinal axis. Nat Rev Neurosci 15:655–669.

Tompary A, Davachi L (2017) Consolidation promotes the emergence of representational overlap in the hippocampus and medial prefrontal cortex. Neuron 96:228–241.e5.

Tukey JW (1949) Comparing individual means in the analysis of variance. Biometrics 5:99–114.

Viganò S, Piazza M (2021) The hippocampal-entorhinal system represents nested hierarchical relations between words during concept learning. Hippocampus 31:557–568.

Voets NL, Zamboni G, Stokes MG, Carpenter K, Stacey R, Adcock JE (2014) Aberrant functional connectivity in dissociable hippocampal networks is associated with deficits in memory. J Neurosci 34:4920–4928.

Wang S-F, Ritchey M, Libby LA, Ranganath C (2016) Functional connectivity based parcellation of the human medial temporal lobe. Neurobiol Learn Mem 134 Pt A:123–134.

Zarei M, Beckmann CF, Binnewijzend MAA, Schoonheim MM, Oghabian MA, Sanz-Arigita EJ, Scheltens P, Matthews PM, Barkhof F (2013) Functional segmentation of the hippocampus in the healthy human brain and in Alzheimer's disease. Neuroimage 66:28–35.

Zeidman P, Maguire EA (2016) Anterior hippocampus: the anatomy of perception, imagination and episodic memory. Nat Rev Neurosci 17:173–182.